Molecular Pharmacology Fast Forward. Published on November 15, 2017 as DOI: 10.1124/mol.117.110007
This article has not been copyedited and formatted. The final version may differ from this version.

Molecular Imaging of GLUT1 and GLUT5 in Breast Cancer: A Multitracer PET Imaging Study in Mice

Melinda Wuest, Ingrit Hamann, Vincent Bouvet, Darryl Glubrecht, Alison Marshall, Brendan Trayner, Olivier-Mohamad Soueidan, Daniel Krys, Michael Wagner, Chris Cheeseman, Frederick West, Frank Wuest

Department of Oncology and Cross Cancer Institute (M.W., I.H., V.B., D.G., A.M., D.K., M.Wa., F.W.) and Department of Chemistry (O.S., F.We.) and Department of Physiology (O.S., B.T., C.C) of University of Alberta, Edmonton, AB, Canada

Molecular Pharmacology Fast Forward. Published on November 15, 2017 as DOI: 10.1124/mol.117.110007
This article has not been copyedited and formatted. The final version may differ from this version.

Running Title: Imaging GLUT1 and GLUT5 in Breast Cancer

Corresponding author: Melinda Wuest
Dept. of Oncology, University of Alberta
11560 University Avenue
Edmonton, AB, T6G 1Z2, Canada
Tel.: +1-780-432-8430
Fax: +1-780-432-8483
Email: mwuest@ualberta.ca

Number of text pages: **26**

Number of tables: **0**

Number of figures: **7**

Number of references: **52**

Number of words: Abstract **256**
Introduction **740**
Discussion **1787**

Non-standard abbreviations:

BC, breast cancer; PET, positron emission tomography; 1-[^{18}F]FDF, 1-deoxy-1-[^{18}F]fluoro-D-fructose; 6-[^{18}F]FDF, 6-deoxy-6-[^{18}F]fluoro-D-fructose; 1-[^{18}F]FDAM, 1-deoxy-1-[^{18}F]fluoro-2,5-anhydromannitol; 6-[^{18}F]FDG, 6-deoxy-6-[^{18}F]fluoro-D-glucose; 2-[^{18}F]FDG, 2-deoxy-6-[^{18}F]fluoro-D-glucose; GLUT1, facilitative glucose transporter 1; GLUT2, facilitative glucose transporter 2; GLUT5, facilitative glucose transporter 5

Molecular Pharmacology Fast Forward. Published on November 15, 2017 as DOI: 10.1124/mol.117.110007
This article has not been copyedited and formatted. The final version may differ from this version.

Abstract

Use of [^{18}F]FDG-PET in clinical breast cancer (BC) imaging is limited mainly due to insufficient expression levels of GLUT1 in up to 50% of all patients. Fructose-specific facilitative hexose transporter GLUT5 represents an alternative biomarker for PET imaging of hexose metabolism in BC. The goal of the present study was to compare uptake characteristics of selected hexose-based PET radiotracers in murine BC model EMT6. Uptake of 1-deoxy-1-[^{18}F]fluoro-D-fructose (1-[^{18}F]FDF), 6-deoxy-6-[^{18}F]fluoro-D-fructose (6-[^{18}F]FDF), 1-deoxy-1-[^{18}F]fluoro-2,5-anhydro-mannitol (1-[^{18}F]FDAM), 2-deoxy-2-[^{18}F]fluoro-D-glucose (2-[^{18}F]FDG) and 6-deoxy-6-[^{18}F]fluoro-D-glucose (6-[^{18}F]FDG) was studied in EMT6 cells, tumors and muscle and correlated to GLUT1 and GLUT5 expression levels. Fructose-derivative 6-[^{18}F]FDF revealed higher tumor uptake than structural analog 1-[^{18}F]FDF while 1-[^{18}F]FDAM with locked anomeric configuration showed similar low tumor uptake as 1-[^{18}F]FDF. Glucose-derivative 6-[^{18}F]FDG reached maximum tumor uptake at 20 min with no further accumulation over time. Uptake of 2-[^{18}F]FDG was highest and continuously increasing due to metabolic trapping through phosphorylation by hexokinase II. In EMT6 tumors, GLUT5 mRNA expression was 20,000-fold lower compared to GLUT1. While latter one was much higher in tumor than in muscle tissue (GLUT1 50:1), opposite was found for GLUT5 mRNA expression (GLUT5 1:6). GLUT5 protein levels were higher in tumor versus muscle tissue as determined by Western Blot and immunohistochemistry. Our data suggest that tumor uptake of fructose metabolism-targeting radiotracers 1-[^{18}F]FDF, 6-[^{18}F]FDF and 1-[^{18}F]FDAM does not correlate with GLUT5 mRNA levels but link to GLUT5 protein levels. In conclusion, our results highlight the importance of detailed biochemical studies on GLUT protein

Molecular Pharmacology Fast Forward. Published on November 15, 2017 as DOI: 10.1124/mol.117.110007
This article has not been copyedited and formatted. The final version may differ from this version.

expression levels in combination with PET imaging studies for functional characterization of GLUTs in BC.

Molecular Pharmacology Fast Forward. Published on November 15, 2017 as DOI: 10.1124/mol.117.110007
This article has not been copyedited and formatted. The final version may differ from this version.

Introduction

Breast cancer (BC) is the most common malignancy in females (Siegel et al., 2017). Specific biomarkers have become important for patient selection and personalized targeted treatment decisions based on precision medicine concept (Jameson and Longo, 2015). In addition to tissue sampling-based biomarker assays, functional molecular imaging with positron emission tomography (PET) can also serve as a biomarker for disease diagnosis and prognosis, and for guiding treatment decisions. The important role of PET imaging for BC management has been summarized in recent reviews (Chudgar and Mankoff, 2017; Kurihara et al., 2016; Lebron et al., 2015; Oude-Munnink et al., 2009; Ulaner et al., 2016).

Among available PET agents, 2-deoxy-2-[^{18}F]fluoro-D-glucose (2-[^{18}F]FDG) is the only FDA approved radiotracer for monitoring BC treatment in primary and metastatic disease (Humbert et al., 2015). However, [^{18}F]FDG-PET also demonstrated variable sensitivity in BC detection, depending on histological tumor type. Regulatory bodies and numerous studies do not recommend [^{18}F]FDG-PET as a standard procedure for BC diagnosis and disease staging in primary invasive BC (Avril et al., 2001; Lebron et al., 2015; Oude-Munnink et al., 2009).

Increased uptake of 2-[^{18}F]FDG is mainly based on overexpression of facilitative hexose transporter GLUT1 in cancer cells (Avril et al., 2001; Brown et al., 1996; Jadvar et al., 2009; Yamamoto et al., 1990). However, variable sensitivity and specificity of [^{18}F]FDG-PET in certain cancers, including BC, have limited its usefulness in both primary and metastatic disease (Gallamini et al., 2014; Kitajima et al., 2016). About 28-47% of BC patients are GLUT1-negative or do not show elevated GLUT1 expression sufficient for 2-

Molecular Pharmacology Fast Forward. Published on November 15, 2017 as DOI: 10.1124/mol.117.110007
This article has not been copyedited and formatted. The final version may differ from this version.

[^{18}F]FDG uptake (primary lesions with ~50% metastatic disease - Kuo et al., 2006; primary lesions - Laudanzki et al., 2004; primary lesions with negative lymph nodes - Ravazoula et al., 2003; primary lesions with higher grade - Younes et al., 1995). Functional changes in 2-[^{18}F]FDG uptake do not correlate with changes in GLUT1 expression in primary BC (Avril et al., 2001). They rather occur due to a complex interaction between cellular energy demand and tumor microenvironment. Therefore, alternative biomarkers of tumor metabolism are of interest for BC. The class II hexose transporter GLUT5, responsible for transport of fructose across cell membranes, represents such an alternative biomarker.

GLUT2 and GLUT5 are primarily responsible for fructose transport across cell membranes (Macheda et al., 2005; Manolescu et al., 2007). They significantly differ in their affinity for fructose (GLUT5 (6mmol/L)>>GLUT2 (76mmol/L) (Barron et al., 2016). In 1996, GLUT5 was first proposed as a novel target for diagnosis and treatment of BC (Zamora-Leon et al. 1996) followed by confirmation of elevated GLUT5 protein expression in BC (Godoy et al. 2006). This has prompted development of various fluorescence- and radio-labeled fructose derivatives targeting GLUT5 (Haradahira et al., 1995; Levi et al., 2007; Tanasova et al., 2013; Trayner et al., 2009; Wuest et al., 2011). Fructose derivative 1-deoxy-1-[^{18}F]fluoro-D-fructose (1-[^{18}F]FDF) was the first PET radiotracer studied in a fibrosarcoma tumor model (Haradahira et al., 1995) but no GLUT5 levels were analyzed. Two fluorescent fructose-derivatives (1-NBDF and 1-Cy5.5-DF) showed good uptake in various BC cells, and 1-NBDF uptake corresponded with fructose uptake (Levi et al., 2007).

Molecular Pharmacology Fast Forward. Published on November 15, 2017 as DOI: 10.1124/mol.117.110007
This article has not been copyedited and formatted. The final version may differ from this version.

Our group developed fructose derivative 6-deoxy-6-fluoro-D-fructose (6-FDF) which accumulated in GLUT5-expressing BC cells (Trayner et al., 2009). Evaluation of ^{18}F-labeled 6-FDF (6-[^{18}F]FDF) demonstrated fructose-mediated uptake in different BC cells and tumors (Wuest et al., 2011). In contrast to 1-[^{18}F]FDF, 6-[^{18}F]FDF displayed efflux from BC cells indicative of no intracellular metabolic trapping as confirmed by phosphorylation experiments with ketohexokinase and hexokinase II. 6-[^{18}F]FDF is a substrate of ketohexokinase but not of hexokinase II. Fluorescent 2,5-anhydro-D-mannitol derivative (NBDM) was tested for GLUT5 transport selectivity over GLUT2 in BC cells (Tanasova et al., 2013). In parallel, our group analyzed fluorinated 2,5-anhydro-D-mannitol derivative (1-FDAM) which possesses GLUT5-mediated uptake into BC cells (Soueidan et al., 2015). Recent analysis of GLUT5 mRNA in BC cells, including knock-down experiments of GLUT5 expression using RNA interference and immunocytochemistry, revealed that GLUT5 may not be the only transporter essential for fructose uptake in BC cells and tissue (Gowrishankar et al., 2011).

The goal of this study was to further analyze if radiolabeled fructose analogues can be used as metabolic radiotracers for molecular imaging of GLUT5 in BC. We *(A)* studied tumor uptake of various ^{18}F-labeled fructose, 2,5-anhydro-D-mannitol and glucose derivatives (1-[^{18}F]FDF, 6-[^{18}F]FDF, 1-[^{18}F]FDAM, 2-[^{18}F]FDG and 6-[^{18}F]FDG) in well-characterized mammary tumor model EMT6 *in vitro* and *in vivo*, and *(B)* correlated uptake of radiotracers with GLUT5 mRNA and protein expression levels in EMT6 cells, tumor and muscle tissue.

Molecular Pharmacology Fast Forward. Published on November 15, 2017 as DOI: 10.1124/mol.117.110007
This article has not been copyedited and formatted. The final version may differ from this version.

Materials and Methods

Chemical and radiochemical syntheses

Non-radioactive compounds for cellular inhibition experiments were prepared according to literature (1-FDF: Haradahira et al., 1995); (3-FDF, 6-FDF and 1-FDAM: Soueidan et al., 2015, Wuest et al., 2011); (6-FDG: Neal et al., 2005). Radiotracer 2-[^{18}F]FDG was prepared at the Edmonton PET Center of the Cross Cancer Institute using a GE TracerLab MX automated synthesis unit. Synthesis of radiotracers 1-[^{18}F]FDAM, 1-[^{18}F]FDF, 6-[^{18}F]FDF and 6-[^{18}F]FDG was carried out based on procedures reported in the literature (Bouvet et al, 2014; Neal et al., 2005; Niu et al., 2013; Haradahira et al., 1995).

GLUT5 inhibitor MSNBA (*N*-(4-methanesulfonyl-2-nitrophenyl)-2H-1,3-benzodioxol-5-amine) was synthesized as following: 3,4-(Methylenedioxy)aniline (1.37 g, 10 mmol) and 1-Fluoro-4-methansulfonyl-2-nitrobenzene (2.19 g, 10mmol) were heated to reflux in water (50 mL). After 40 min (TLC), Na_2CO_3 (1.8 g) was carefully added and the reaction mixture was cooled to room temperature. The crude product was filtered off and the aqueous phase was extracted with EtOAc. The combined organic extracts including the crude product were dried over Na_2SO_4 and the solvent was removed in vacuo. The dark residue was purified using flash chromatography (SiO_2, EtOAc/Hexane 1:2→2:1). The obtained red solid was recrystallized from EtOAc/EtOH/Hexane to give an orange solid that was dried in vacuo. Yield: 64.7 % (2.175 g, 6.47 mmol), mp. > 154°C (decomp.), HPLC: >98 % purity (@280 nm), R_f (hexane/ethylacetate 1:1) = 0.36, **^{1}H NMR** (600.27 MHz, $(CD_3)_2S=O$): δ 9.81 (s, 1H), 8.54 (d, J = 2.3 Hz, 1H), 7.86 (dd, J = 1.9 Hz, J = 9.0 Hz, 1H), 7.07 (d, J = 9.0 Hz, 1H), 7.01 (d, J = 9.0 Hz, 1H), 6.97 (d, J= 1.9 Hz), 6.84 (dd,

Molecular Pharmacology Fast Forward. Published on November 15, 2017 as DOI: 10.1124/mol.117.110007
This article has not been copyedited and formatted. The final version may differ from this version.

J = 1.9 Hz, *J* = 7.9 Hz, 1H), 6.02 (s, 2H, CH_2), 3.21 (s, 3H, CH_3);**^{13}C NMR** (150.94 MHz,$(CD_3)_2S=O$): δ 148.1 (C quart.),146.6 (C quart.), 146.1 (C quart.), 133.3 (C-H), 131.7 (C quart.), 131.0 (C quart.), 126.8 (C-H), 119.7 (C-H), 117.3 (C-H), 108.8 (C-H), 107.6 (C-H), 101.7 (CH_2), 43.7 (CH_3); **ESI MS** (CH_3CN, +): *m/z* 337.0 ($[M+H]^+$, 100%); **ESI MS** (CH_3CN, −): *m/z* 335.0 ($[M-H]^+$, 100%); **UV/Vis** (Acetonitrile): λ_{max} (ε): 410 nm (4360 $Lmol^{-1}cm^{-1}$), 280 nm (11140 $Lmol^{-1}cm^{-1}$). The ^{1}H NMR spectrum of the GLUT-5 inhibitor confirmed the commercially available compound (Enamine Ltd, Kiev, Ukraine) as reported by George Thompson et al. (2016). MSNBA was soluble at 150 µmol/L in 1% DMSO/H_2O.

Cell culture

Murine mammary gland tumor cells EMT6 (ATTC® CRL-2755™) and human BC cells MDA-MB231 (ATCC® HTB-26™) were grown in a CO_2 incubator at 37°C, in Gibco® DMEM/F-12 supplemented with 10% fetal bovine serum (GIBCO, 12483) and 1% penicillin/streptomycin and split every 2-3 days.

mRNA expression of GLUT-1 and GLUT-5

Total RNA was isolated from EMT6 cells, EMT6 tumor tissue and mouse muscles tissue by using the TRIzol® Plus RNA Purification Kit (Applied Biosystems, Life Technologies, Burlington, ON, Canada). EMT6 cells were harvested using TRIzol® reagent, while tissues were excised from euthanized mice and immediately frozen in liquid nitrogen. Samples were stored at -80°C.

Molecular Pharmacology Fast Forward. Published on November 15, 2017 as DOI: 10.1124/mol.117.110007
This article has not been copyedited and formatted. The final version may differ from this version.

At a later date, tissues were pulverized, using a mortar and pestle containing liquid nitrogen and re-suspended in the provided lysis buffer of the purification kit. RNA from cells and tissues was purified according to the manufacturer's instructions and stored at -80°C. RNA was reverse-transcribed into cDNA using the High-Capacity cDNA reverse transcription kit (Applied Biosystems, Life Technologies, Burlington, ON, Canada) according to the manufacturer's instructions. Quantitation of GLUT1, GLUT2, GLUT5 and 18 sRNA mRNA levels were performed by real-time PCR, employing specific TaqMan® gene expression assays (Applied Biosystems, Life Technologies, Burlington, ON, Canada) using probes 5'-labeled with 6-FAM and 3' with MGBNFQ (Minor groove binder/Non-fluorescent quencher). The following TaqMan® gene expression assays were employed: GLUT1 (Mm00441480_m1), GLUT2 (Mm00446229_m1), GLUT5 (Mm00600311_m1) and, as an internal control, 18 sRNA (Mm039288990_g1).

Cycling conditions were the manufacturer's recommended default values (1 cycle of 2 minutes at 50°C and 10 minutes at 95°C, then 40 cycles of 15 s at 95°C and 1 minute at 60°C) and performed on a CFX Connect™ Real-Time PCR Detection System (Biorad, Mississauga, ON, Canada).

Real-time PCR data was analyzed using relative gene expression as described before (Livak and Schmittgen 2001; Pfaffl 2001). For each sample, a threshold cycle (C_T) was calculated based on the time (measured by the number of PCR cycles) at which the reporter fluorescence emission increased beyond a threshold level based on the background fluorescence of the system. Triplicate measurements were done for each sample in three independent experiments. Results were expressed using the comparative C_T method with 18s RNA as the housekeeping gene, which was investigated with the

Molecular Pharmacology Fast Forward. Published on November 15, 2017 as DOI: 10.1124/mol.117.110007
This article has not been copyedited and formatted. The final version may differ from this version.

genes of interest in order to rule out variations due to pipetting, cDNA synthesis, PCR reaction etc. and C_T values for the genes of interest were normalized to the C_T values of 18s RNA. Relative differences in the expression level of the two genes of interest were calculated in the following manner:

$R = (2^{(C_T \text{ GLUT1} - C_T \text{ GLUT5})}) / (2^{(C_T \text{ 18s RNA for GLUT1} - C_T \text{ 18s RNA for GLUT5})})$ in Figure 3A or

$R = (2^{(C_T \text{ GLUT tumor} - C_T \text{ GLUT muscle})}) / (2^{(C_T \text{ 18s RNA for GLUT tumor} - C_T \text{ 18s RNA for GLUT muscle})})$

GLUT5 protein expression

Western blots for detection of GLUT5 protein levels were carried out with tumor and muscle tissues of EMT6 tumor-bearing BALB/c mice. Tissues were excised from euthanized mice and immediately frozen in liquid nitrogen. Samples were stored at -80°C. At a later date, tissues were pulverized, using a mortar and pestle, containing liquid nitrogen and re-suspended in lysis buffer (50 mM Tris, 150 mM NaCl, 0.1% SDS, 0.5% sodium deoxycholate, 0.5% Triton X). After cell lysis on ice for 30 min, extracts were sonicated (10% amplitude, 10 s) on ice and centrifuged at 13,500 g for 10 min at 4°C to remove debris. Protein determination in supernatants was conducted using a BCA based protein assay (Pierce/Thermo Scientific, Rockford, USA). Aliquots of the supernatants were mixed with 1/4 volume of 4x Laemmli buffer (250 mMTris/HCl, 8% (w/v) SDS, 40% glycerol, 200 mM dithiothreitol and 0.04% (w/v) bromophenol blue, pH 6.8) and heated for 5 min at 95°C. The protein extracts were applied to SDS-polyacrylamide gels and separated by electrophoresis. Proteins were transferred to nitrocellulose membranes by electroblotting and blocked for 1 h at room temperature in 5% (w/v) non-fat dry milk in Tris-buffered saline containing 0.05% (v/v) of Tween-20 (TBST). Membranes were

Molecular Pharmacology Fast Forward. Published on November 15, 2017 as DOI: 10.1124/mol.117.110007
This article has not been copyedited and formatted. The final version may differ from this version.

incubated overnight at 4°C with the following primary antibodies: mouse monoclonal anti-GLUT5 IgG1 (clone E2, sc-271055, Santa Cruz Biotechnology, Dallas, TX, USA, 1:500) and mouse anti-α-tubulin (12G10, Developmental Studies Hybridoma Bank, 1:50000) followed by incubation for 1 h at room temperature with a peroxidase-conjugated anti-mouse IgG1 secondary antibody (sc-2060, Santa Cruz Biotechnology) in 1:5000 dilution and 100000 dilution, respectively.

After incubation with secondary antibodies, membranes were washed in TBST and depending on protein levels incubated with Thermo Scientific SuperSignal West Pico Chemiluminescent Substrate (Thermo scientific) or Clarity™ ECL Western Blotting Substrate (Biorad). Luminescence signals were captured, using Fuji medical Xray films (Fuji). Films were scanned and analysis was done, using the ImageJ program. Density of each band was determined and individual lane backgrounds subtracted. Values for GLUT5 protein were divided by values, for the housekeeping protein α-tubulin. Received values for each individual muscle were set 100% and compared with the individual value of the respective tumor tissue (band density Glut5 - density lane background) / (band density α-tubulin-density lane background), respectively.

In vitro inhibition of 6-[^{18}F]FDF and 2-[^{18}F]FDG cell uptake

To estimate the affinity of non-radiolabeled fructose derivatives (1-,3- and 6-FDF) as well as the 2,5-anhydro-D-mannitol 1-FDAM for fructose mediated transport in comparison to that of D-fructose itself, ranges for half-maximum inhibition coefficients (IC_{50}) values of both compounds were estimated.

Molecular Pharmacology Fast Forward. Published on November 15, 2017 as DOI: 10.1124/mol.117.110007
This article has not been copyedited and formatted. The final version may differ from this version.

EMT6 cells were incubated with glucose-free Krebs-Ringer buffer containing 6-[^{18}F]FDF and different concentrations of either 1-FDF, 6-FDF, 3-FDF, 1-FDAM (10^{-8} –10^{-3} – $3x10^{-2}$ M) or fructose (10^{-5} - 1 M) and no compound at all for comparison (= 100% uptake). After 60 min cells were rinsed with ice-cold Krebs-Ringer solution, lysed and counted in a γ-counter as described below. Increasing concentrations of glucose were analyzed on 6-[^{18}F]FDF uptake (60min incubation) in MDA-MB 231 cells, increasing concentrations of fructose as well cytochalasin B (10^{-7}-$3x10^{-5}$M) against 2-[^{18}F]FDG uptake. Novel selective GLUT5 inhibitor MSNBA (100-300µM in Krebs-buffer 1% DMSO) was analyzed on 6-[^{18}F]FDF and 2-[^{18}F]FDG uptake into murine EMT6 cells.

In vitro cell uptake of ^{18}F-labeled radiotracers

For radiotracer uptake studies, cells were grown to confluence in 12-well plates using in Gibco® DMEM/F-12 medium (containing 10% fetal bovine serum (GIBCO, 12483) and 1% penicillin/streptomycin). One hour prior to the experiment, the media was removed and the cells were washed two times with phosphate-buffered saline solution (PBS). Next, glucose-free Krebs-Ringer solution (120 mM NaCl, 4 mM KCl, 1.2 mM KH_2PO_4, 2.5 mM $MgSO_4$, 25 mM $NaHCO_3$, 70 µM $CaCl_2$, pH 7.4) was added to the cells. 300 µl Krebs-Ringer (with or without 5 mM glucose or 30 mM fructose) solution with 0.1-0.5 MBq ^{18}F-labeled radiotracer was added to each well and the plates were incubated at 37°C for specific periods of time (5, 10, 15, 30, 45 and 60 min). Radiotracer uptake was stopped with 1mL ice-cold PBS, the cells were washed twice with PBS and lysed in 0.4mL radioimmunoprecipitation assay buffer (RIPA buffer). Radioactivity in the cell lysates was determined as counts per minute [CPM] using a WIZARD2 Automatic gamma counter

Molecular Pharmacology Fast Forward. Published on November 15, 2017 as DOI: 10.1124/mol.117.110007
This article has not been copyedited and formatted. The final version may differ from this version.

(Perkin Elmer; Waltham, MA, USA) and converted to the radioactivity dose SI unit Bequerel [Bq]. Total protein concentration in the samples was determined by the bicinchoninic acid method (BCA; Pierce, Thermo Scientific 23227) using bovine serum albumin as protein standard. Data were calculated as percent of measured radioactivity per mg protein (%radioactivity / mg protein). Cell uptake of 6-[^{18}F]FDF and 2-[^{18}F]FDG after 60 min incubation time was compared in murine EMT6 versus human MDA-MB231 BC cells. Graphs were constructed using GraphPad Prism 5.0 (GraphPad Software). Statistical differences were tested by unpaired Student's t-test and were considered significant for $p<0.05$. Data in Figure 2B) was statistically analyzed with one-way ANOVA plus Bonferroni post test and considered significant for $p<0.05$.

Animal model

All animal experiments were carried out in accordance with guidelines of the Canadian Council on Animal Care (CCAC) and were approved by the local animal care committee of the Cross Cancer Institute.

Murine EMT6 cells (1 x 10^6 cells in 100 μl PBS) were injected into the upper left shoulder of 4-6 month old female BALB/c mice (20-24 g, Charles River, Saint-Constant, Quebec, Canada). The EMT6 tumor-bearing mice were imaged after allowing 7 to 11 days of tumor growth reaching sizes of ~300-400 mm^3. The mice were not fasted prior to imaging experiments.

Immunohistochemistry GLUT5

Molecular Pharmacology Fast Forward. Published on November 15, 2017 as DOI: 10.1124/mol.117.110007
This article has not been copyedited and formatted. The final version may differ from this version.

Excised tissues from euthanized mice were fixed in neutral buffered 10% formalin overnight and embedded in paraffin. Sections of 4 µm thickness were dried in an oven at 60°C for 1 hour. Sections were rehydrated by placing the slides in three changes of xylene for 10 min each, then graded ethanol from 100% to 50%, followed by water and TBS. Slides were microwaved in a pressure cooker for 6 min in citraconic anhydride (0.05% in water, pH 7.4) for antigen retrieval. Slides were blocked with 0.5% fish gelatin in Tris-buffered saline with 0.05% Tween-20 (TBST) for 30 min and incubated with mouse monoclonal anti-GLUT5 antibody (clone E2, sc-271055, Santa Cruz Biotechnology, 1:50) in a humidity chamber overnight at 4°C. After incubation in 3% H_2O_2 in water for 15 minutes, slides were incubated with DakoCytomation Envision+ anti-mouse Labelled Polymer HRP (DakoCytomation, Glostrup, Denmark) for 1h, developed, using Dako Liquid DAB+ Substrate Chromagen System and 1% copper sulfate and counterstained with hematoxylin.

Slides were dehydrated by reversing re-hydration procedure and cover-slipped. Negative control was provided by omitting the GLUT5 primary antibody, while positive control was provided by examining sections of murine small intestine, a tissue known to express GLUT5.

In vivo PET experiments

EMT6 tumor bearing BALB/c mice were anesthetized with isoflurane in 40% oxygen / 60% nitrogen (gas flow, 1 L/min) and body temperature was kept constant at 37°C for the entire experiment. Mice were positioned and immobilized in the prone position into the centre of the field of view of an INVEON® PET scanner (Siemens

Molecular Pharmacology Fast Forward. Published on November 15, 2017 as DOI: 10.1124/mol.117.110007
This article has not been copyedited and formatted. The final version may differ from this version.

Preclinical Solutions, Knoxville, TN, U.S.A.). A transmission scan for attenuation correction was not acquired. The amount of radioactivity [Bq] present in the injection solution in a 0.5 mL syringe was determined with a dose calibrator (Atomlab^{TM} 300, Biodex Medical Systems, New York, U.S.A.). After emission scan was started, radioactivity was injected with a delay of approximately 15 s. Data acquisition continued for 120 min in 3D list mode. 4-8 MBq of ^{18}F-labeled radiotracer in 100 -150 μL saline was injected through a tail vein catheter. The list mode data were sorted into sinograms with 59 time frames (10 x 2 s, 8 x 5 s, 6 x 10 s, 6 x 20 s, 8 x 60 s, 10 x 120 s, 10 x 300 s). The frames were reconstructed using the Ordered Subset Expectation Maximization (OSEM) or maximum a posteriori (MAP) reconstruction modes. No correction for partial volume effects was performed. The image files were further processed using the ROVER v2.0.51 software (ABX GmbH, Radeberg, Germany).

Masks defining 3D regions of interest (ROI) were set and the ROIs were defined by thresholding. ROIs covered all visible tumor mass of the subcutaneous tumors, and the thresholds were defined by 50% of the maximum radioactivity uptake level for each EMT6 tumor in each animal. Mean standardized uptake values [SUV_{mean} = (activity [Bq]/mL tissue)/(injected activity [Bq]/body weight), mL/kg] were calculated for each ROI. Time-activity curves (TAC) were generated from the dynamic scans. All semi-quantified PET data are presented as means ± SEM. Time-activity curves were constructed using GraphPad Prism 5.0 (GraphPad Software). Statistical differences were tested by paired (comparing tumor and muscle uptake in the same mice) and unpaired Student's t-test and were considered significant for $p<0.05$. Tumor-to-muscle ratios in Figure 7 were

Molecular Pharmacology Fast Forward. Published on November 15, 2017 as DOI: 10.1124/mol.117.110007
This article has not been copyedited and formatted. The final version may differ from this version.

statistically analyzed with one-way ANOVA plus Bonferroni post test and considered significant for $p<0.05$.

Results

Figure 1 displays the structures all ^{18}F-labeled fructose, glucose and 2,5-anhydro-D-mannitol derivatives used for the present study. All radiotracers were obtained at high radiochemical purity (>95%) and high volume activities suitable for all subsequent *in vitro* and *in vivo* experiments.

Cellular uptake studies

Two different cellular uptake studies were carried out using murine mammary gland tumor cell line EMT6. The first set of experiments involved inhibition studies of radiotracer 6-[^{18}F]FDF in the presence of D-fructose, fructose derivatives 1-FDF, 3-FDF and 6-FDF, and 2,5-anhydro-D-mannitol derivative 1-FDAM according to a procedure developed by our research group (Wuest et al. 2011). Uptake of radiotracer 6-[^{18}F]FDF into EMT6 cells was competitively inhibited using increasing concentrations of non-radiolabeled compounds. Based on the inherent limitations of the assay with regard to the high concentrations of non-radiolabeled compounds (>100mM), it was only possible to estimate half-maximum inhibition concentration (IC_{50}) ranges (**Figure 2** A).

As measured estimated IC_{50} values for 1-FDF, 3-FDF and 1-FDAM should be in a similar range as the one for 6-FDF. Therefore all analyzed fructose derivatives may more potent then fructose itself. However, this was measured competing against 6-[^{18}F]FDF and not

Molecular Pharmacology Fast Forward. Published on November 15, 2017 as DOI: 10.1124/mol.117.110007
This article has not been copyedited and formatted. The final version may differ from this version.

radiolabeled fructose. IC_{50} values for the inhibition of 6-[^{18}F]FDF uptake in EMT6 cells have previously been reported for 6-FDF (19mM) and D-fructose (322mM) (Wuest et al. 2011). The results were reproduced in the present study.

A second experimental setup analyzed direct uptake pattern of ^{18}F-labeled fructose and 2,5-andydromannitol derivatives 1-[^{18}F]FDF, 6-[^{18}F]FDF and 1-[^{18}F]FDAM into EMT6 cells in comparison with glucose derivatives 2-[^{18}F]FDG and 6-[^{18}F]FDG (**Figure 2B**). 6-[^{18}F]FDF reached a cellular uptake level of 26 ± 3 % radioactivity/mg protein (n=9) after 60 min, whereas uptake values for 1-[^{18}F]FDF and 1-[^{18}F]FDAM were significantly lower (5.5 ± 0.5 (n=9; $p < 0.001$) and 3 ± 0.1 % radioactivity/mg protein (n=3; $p < 0.001$)). Glucose derivatives 2-[^{18}F]FDG displayed very high uptake levels of 622 ± 25 % radioactivity/mg protein (n=3) whilst 6-[^{18}F]FDG only showed very low cellular uptake of 2.2 ± 0.3 % radioactivity/mg protein (n=3).

The observed differences in cellular uptake levels demonstrate the importance of stereochemistry and substitution pattern for recognition and transport of radiotracers 1-[^{18}F]FDAM, 1-[^{18}F]FDF, 6-[^{18}F]FDF, 2-[^{18}F]FDG and 6-[^{18}F]FDG by hexose transporters GLUT1 and GLUT5. This is consistent with recent finding by our group using fluorescent hexose derivatives (Soueidan et al., 2017).

In addition, cellular uptake of glucose derivative 2-[^{18}F]FDG was analyzed in the presence of glucose, fructose and cytochalasin B (**Figure 2C**) as well as effect of glucose on 6-[^{18}F]FDF uptake (**Figure 2D**). The IC_{50} values for fructose against 2-[^{18}F]FDG uptake revealed 80mM in EMT6 cells and 210mM in MDA-MB231 cells which represents a similar order of magnitude compared to inhibition of 6-[^{18}F]FDF (~320mM, see above). Glucose had a 3 orders of magnitude lower IC_{50} against 6-[^{18}F]FDF: 117mM (as

Molecular Pharmacology Fast Forward. Published on November 15, 2017 as DOI: 10.1124/mol.117.110007
This article has not been copyedited and formatted. The final version may differ from this version.

determined in human MDA-MB231 cells) versus 0.22mM (measured in murine EMT6 cells) against 2-[^{18}F]FDG uptake. Cellular uptake of both the glucose derivative 2-[^{18}F]FDG and the fructose derivative 6-[^{18}F]FDF was slightly higher in murine EMT6 versus human MDA-MB231 BC cells (**Figure 2E**) but showed a similar ratio between glucose- and fructose-mediated uptake levels. Cytochalasin B (30µM) inhibited 100% 2-[^{18}F]FDG uptake but also ~50% of 6-[^{18}F]FDF uptake indicative for a potential functional involvement of GLUT2 and/or GLUT4 (**Figure 2F**). Effects of novel selective GLUT5 inhibitor MSNBA were analyzed against 6-[^{18}F]FDF (**Figure 2H**) and 2-[^{18}F]FDG (**Figure 2G**) uptake and compared with effects of glucose and fructose. MSNBA had only very minor inhibition effects using up to 300µM concentration which was limited by further solubility and DMSO concentration for the cell assay.

Expression levels of GLUT1 and GLUT5 mRNA in EMT6 cells, EMT6 tumors and mouse muscle tissue

Expression of GLUT1 and GLUT5 mRNA was determined in EMT6 cells, EMT6 tumors and mouse muscle tissue. In addition, GLUT1 and GLUT5 mRNA levels were compared in tumor and muscle tissue (**Figure 3**).

In comparison to GLUT5, mRNA levels of GLUT1 were about 76,000 times higher in EMT6 cells, about 20,000 times higher in EMT6 tumors and about 45 times higher in muscle tissue. This result indicated that GLUT5 mRNA levels were always significantly lower compared to GLUT1 mRNA levels. In tumor tissue, GLUT1 mRNA levels were about 1.7 times and GLUT5 mRNA levels about 2.4 times higher compared to EMT6 cells. Direct comparison of GLUT1 mRNA levels in tumor and muscle tissue revealed a 60 times

Molecular Pharmacology Fast Forward. Published on November 15, 2017 as DOI: 10.1124/mol.117.110007
This article has not been copyedited and formatted. The final version may differ from this version.

higher expression of GLUT1 mRNA in tumor tissue. Unlike to GLUT1 mRNA levels, tumor tissue expressed about 6 times less GLUT5 mRNA than muscle tissue.

Protein expression of GLUT5 in EMT6 tumors and muscle tissue

Western Blot analyses of GLUT5 expression in tumor and muscle tissue were performed to correlate determined GLUT5 mRNA levels with GLUT5 protein levels (**Figure 4**). Surprisingly and in contrast to the PCR analyses, GLUT5 protein levels were highest in tumor tissue and about 30% lower in muscle tissues. This finding directs to important and significant differences in GLUT5 mRNA and protein levels in tumor and muscle tissue.

Immunohistochemical determination of GLUT5 in EMT6 tumors and muscle tissue

In addition to Western blot experiments, GLUT5 protein expression levels in tumor and muscle tissue were further analyzed by immunohistochemical staining. Control slides, prepared without anti-GLUT5 antibody, revealed no background immunoperoxidase staining and could therefore be used as GLUT5 negative controls. Positive controls were obtained using mouse intestine samples (**Figure 5**). Murine duodenum tissue is well known to express high levels of GLUT5 (Fatima et al., 2009).

No staining of GLUT5 protein was detected in muscle tissue of two individual mice (**Figure 5**). Examination of tumor tissue from two mice showed for the most of the tumor area negative GLUT5 staining whereas a small region in the centre of both tumors showed high GLUT5 staining. Interestingly, this transition from negative to positive staining seemed to be quite abrupt and staining frequency increased in tumor regions, where cells appeared to undergo pyknosis. In summary, immunohistochemistry analyses clearly

Molecular Pharmacology Fast Forward. Published on November 15, 2017 as DOI: 10.1124/mol.117.110007
This article has not been copyedited and formatted. The final version may differ from this version.

showed GLUT5 protein expression in tumor tissue, while muscle tissue was GLUT5 negative.

PET imaging in EMT6 tumor bearing mice

PET imaging with ^{18}F-labeled radiotracers 1-[^{18}F]FDAM, 1-[^{18}F]FDF, 6-[^{18}F]FDF, 2-[^{18}F]FDG and 6-[^{18}F]FDG in EMT6 tumor bearing mice revealed important differences in tumor and muscle uptake as well as in clearance parameters (blood, liver, kidneys, clearance from non-target tissue muscle).

Figure 6 summarizes all PET images at 15 and 60 min p.i. as collected over 2 h from dynamic PET scans. Tumors were clearly visible after injection of glucose derivative 2-[^{18}F]FDG, whereas the other glucose derivative 6-[^{18}F]FDG resulted in much lower tumor uptake levels. Fructose derivative 6-[^{18}F]FDF showed high initial tumor uptake at 15 min p.i. followed by a washout of radioactivity from tumor tissue over time. However, total tumor uptake after 60 min of 6-[^{18}F]FDF was markedly lower compared to glucose derivatives 2-[^{18}F]FDG and 6-[^{18}F]FDG as seen from the SUV_{60min} values (**Figure 6**) but higher than 1-[^{18}F]FDF and 1-[^{18}F]FDAM. 2,5-Anhydro-D-mannitol derivative 1-[^{18}F]FDAM displayed only low tumor uptake levels with only very little remaining contrast after 60 min p.i.. Fructose derivative 1-[^{18}F]FDF showed lowest tumor uptake and image contrast compared to all other tested ^{18}F-labeled radiotracers.

Figure 7 depicts generated time-activity curves (TACs) for each radiotracer in tumor and muscle tissue over a 2 h time frame as well as the corresponding tumor-to-muscle ratios (**Figure 7, bottom right**). Radiotracers 2-[^{18}F]FDG, 6-[^{18}F]FDG and 6-[^{18}F]FDF showed initial high tumor uptake after 15min p.i. (SUVs 1.01 ± 0.23 (n=4), 1.16 ± 0.13 and

Molecular Pharmacology Fast Forward. Published on November 15, 2017 as DOI: 10.1124/mol.117.110007
This article has not been copyedited and formatted. The final version may differ from this version.

1.08 ± 0.16, both n=3). As expected, tumor uptake of 2-[^{18}F]FDG continued to increase over time reaching a SUV_{120min} 1.97 ± 0.23 (n=4), whereas tumor uptake of 6-[^{18}F]FDF decreased constantly to a SUV_{120min} 0.59 ± 0.06 (n=4). Tumor uptake of glucose derivative 6-[^{18}F]FDG was lower peaking at 35 min p.i. (SUV 1.28 ± 0.05), and was slightly reduced over time (SUV_{120min} 1.14 ± 0.05, n=3). After 2 h p.i. fructose derivative 6-[^{18}F]FDF (SUV_{120min} 0.59 ± 0.06; n=4) resulted in significantly higher tumor uptake compared 1-[^{18}F]FDF (SUV_{120min} 0.31 ± 0.06; n=3; $p<0.05$) and 1-[^{18}F]FDAM (SUV_{120min} 0.28 ± 0.01; n=3; $p<0.01$), respectively. Also, uptake of glucose derivative 2-[^{18}F]FDG (SUV_{120min} 1.97 ± 0.23; n=4) was significantly higher than 6-[^{18}F]FDG (SUV_{120min} 1.14 ± 0.05; n=3; $p<0.05$). A rather unexpected observation was the increasing muscle uptake of 6-[^{18}F]FDG over time since this hexose derivative should not be recognized by hexokinase II and based on that would not undergo any intracellular trapping mechanism as shown for the tumor uptake curve. All other radiotracers (1-[^{18}F]FDAM, 1-[^{18}F]FDF, 6-[^{18}F]FDF and 2-[^{18}F]FDG) showed washout from muscle tissue over time. The increasing muscle uptake of 6-[^{18}F]FDG over time resulted in a decreasing tumor-to-muscle ratio, while tumor-to-muscle ratios of other radiotracers increased over time (**Figure 7, bottom right**). One-way ANOVA with additional Bonferroni post test did not reveal any differences in tumor-to-muscle ratios between 1-[^{18}F]FDAM, 1-[^{18}F]FDF, 6-[^{18}F]FDF and 6-[^{18}F]FDG, only 2-[^{18}F]FDG had a significantly higher value ($p<0.01$) after 2h p.i..

In contrast to fructose derivative 6-[^{18}F]FDF, fructose and 2,5-anhydro-D-mannitol analogues 1-[^{18}F]FDF and 1-[^{18}F]FDAM showed only moderate tumor uptake (SUV_{15min} 1-[^{18}F]FDF 0.47 ± 0.08; 1-[^{18}F]FDAM 0.58 ± 0.10; both n=3) which decreased over time reaching SUV_{120min} of 0.31 ± 0.06 and 0.28 ± 0.01, respectively.

Molecular Pharmacology Fast Forward. Published on November 15, 2017 as DOI: 10.1124/mol.117.110007
This article has not been copyedited and formatted. The final version may differ from this version.

In summary, except for GLUT1 radiotracer 2-[^{18}F]FDG, the highest tumor uptake was observed with fructose analogue 6-[^{18}F]FDF, while other potential GLUT5 radiotracers 1-[^{18}F]FDF and 1-[^{18}F]FDAM showed much lower tumor uptake levels and only minor differences between specific (tumor) and non-specific (muscle) uptake.

Discussion

Glucose analogue 2-[^{18}F]FDG is the most versatile and widely used radiotracer for PET imaging of cancer in the clinic. However, application of [^{18}F]FDG-PET in BC patients has resulted in high non-responder rates and false-positive responses which limit specificity of [^{18}F]FDG-PET for BC imaging (Adeloju et al., 2012). Therefore, alternative biomarkers such as estrogen receptors and HER2 have been introduced for more specific targeted molecular imaging of BC (Dalm et al., 2017; Kenny 2016) being only available at selected and specialized centres and not used routinely.

Shifting from glucose-based to a solely fructose-mediated transport in BC appeared to be an alternative approach to address specificity concerns of the otherwise [^{18}F]FDG-PET dominated clinical practice of BC imaging. Molecular imaging of fructose transport was first proposed in a study by Zamora-Leon who analysed fructose transporter GLUT5 expression in BC (Zamora-Leon et al., 1995). Several subsequent studies described specific targeting of GLUT5 in mammary and human xenograft BC with various fluorescent or radiolabeled fructose and 2,5-anhydro-D-mannitol derivatives as molecular probes (Levi et al., 2007; Soueidan et al., 2015; Soueidan et al., 2017; Tanasova et al., 2013; Trayner et al., 2009; Wuest et al., 2011). To date no systematic and comparative

Molecular Pharmacology Fast Forward. Published on November 15, 2017 as DOI: 10.1124/mol.117.110007
This article has not been copyedited and formatted. The final version may differ from this version.

study has been reported on testing various ^{18}F-labeled hexoses and 2,5-anhydromannitols with respect to their GLUT1- and GLUT5-mediated uptake in target (breast tumor) and reference (muscle) tissue. For this purpose we have selected well-characterized murine mammary gland tumor cell line EMT6 as a suitable preclinical model for this study (Bouvet et al., 2011; Knight et al., 2013; Way et al., 2014; Wuest et al., 2011; Wuest et al., 2015).

GLUT1 expression in EMT6 cells has been confirmed by several 2-[^{18}F]FDG-PET imaging and cell studies (Kelly et al., 2012; Rowland et al., 2005; Wuest et al., 2011). All studies reported high uptake and retention of 2-[^{18}F]FDG in EMT6 cells and tumors consistent with GLUT1-mediated radiotracer uptake and metabolic trapping through phosphorylation by hexokinase II (Wuest et al., 2011). Expression of GLUT5 in BC tissue was reported differently in the literature. Our present results show only low expression of GLUT5 mRNA in EMT6 cells and tumor tissue compared to GLUT1 mRNA levels. Interestingly, GLUT5 mRNA expression was about 6x higher in muscle versus tumor tissue. This is contrary to GLUT1 mRNA levels. Subsequent analysis with Western Blot revealed elevated GLUT5 protein levels in tumor versus muscle tissue. Immunohistochemistry detected GLUT5 protein in tumor tissue only, probably due to limit of detection of this method, using only a very thin slice of the tumor tissue in comparison to Western Blot analysis, where much larger parts of the tumor and muscle tissue were analysed. GLUT5 protein data provided the basis for the multitracer PET imaging study.

Gowrishankar and co-workers (2011) detected higher GLUT5 mRNA levels in “control” mammary cells MCF10A compared to MCF-7 and MDA-MB 468 cells. However, MCF10A is a non-tumorigenic epithelial cell line which has undergone pathophysiological changes,

Molecular Pharmacology Fast Forward. Published on November 15, 2017 as DOI: 10.1124/mol.117.110007
This article has not been copyedited and formatted. The final version may differ from this version.

including inflammation (Soule et al., 1990), making this cell line not ideal as a non-tumor "control" for BC. Immunohistochemistry from the same study detected no elevated GLUT5 protein in BC versus adjacent normal breast tissue. From 40 BC patients, only 35% (14 samples) showed staining of ≥2 for GLUT5 protein on a scale from 0 - 4. The majority showed only weak (24 samples) or no (4 samples) GLUT5 staining (Gowrishankar et al., 2011). This is in contrast to earlier studies demonstrating elevated GLUT5 protein expression levels in BC versus normal breast tissue (Godoy et al., 2006; Zamora-Leon et al., 1996). Our data on GLUT5 protein expression in murine tumor and muscle tissue supports earlier reports describing elevated GLUT5 protein levels in BC tissue (Godoy et al., 2006; Zamora-Leon et al., 1996). However, protein levels of GLUT5 in BC tissues remain unclear, and more studies in different BC patient groups are needed for comprehensive conclusions.

Discrepancy between GLUT5 protein and mRNA expression levels most likely results from complex gene expression biology, which suggests various levels of regulation during protein synthesis, e.g. posttranscriptional, translational, or posttranslational regulation (Tian et al., 2004). Differential mRNA expression can capture at most 40% of protein expression variation. Thus, integrated analysis of both mRNA and protein levels is crucial in complex biological systems like cancer cells. In addition, immunohistochemistry may capture solely skeletal muscle tissue GLUT5 expression at a low level, while western blot analysis using tissue homogenates include a mixture of cells not just skeletal muscle cells. However, GLUT5 was detected on mRNA as well as protein level concluding for some GLUT5 expression in muscle tissue.

Molecular Pharmacology Fast Forward. Published on November 15, 2017 as DOI: 10.1124/mol.117.110007
This article has not been copyedited and formatted. The final version may differ from this version.

EMT6 cell uptake experiments with all used radiotracers revealed only significant uptake of glucose derivative 2-[^{18}F]FDG and fructose analogue 6-[^{18}F]FDF. Both also showed sufficient uptake in human triple-negative BC cancer MDA-MB231 cells indicating that BC cells with elevated glucose metabolism also have a certain level of elevated fructose consumption. This points toward a similar regulation mechanism of glucose and fructose uptake in both murine and human cells which would be relevant for the BC patient situation. Uptake of 6-[^{18}F]FDF was not affected in the presence of 5mM glucose, a concentration which strongly inhibits glucose transport through GLUT1 (Wuest et al., 2011). At glucose concentrations of >10mM effects are detected on 6-[^{18}F]FDF indicative for involvement of a glucose-transporting GLUT. Incorporation of fluorine in 6-position also prevented phosphorylation by hexokinase II as demonstrated by cellular efflux due to lack of metabolic trapping. However, 6-[^{18}F]FDF is a substrate of ketohexokinase (Wuest et al., 2011). There is evidence that ketohexokinase cannot be detected in numerous cancer cells (Hwa et al., 2006; Soueidan et al., 2015; Trayner et al., 2009; Wuest et al., 2011). Interestingly, fructose derivative 1-[^{18}F]FDF, which was reported as a GLUT5 substrate (Haradahira et al., 1995), showed 5x lower uptake into EMT6 cells compared to structurally related 6-[^{18}F]FDF. Presence of the 6-OH group qualifies 1-[^{18}F]FDF as a potential substrate for hexokinase II. Low cell uptake of 1-[^{18}F]FDF versus 6-[^{18}F]FDF is somewhat surprising since both molecules are structural analogues. The only major alteration is the different fluorine-labeling position. As for all hexoses, fructose derivatives 1-[^{18}F]FDF and 6-[^{18}F]FDF can form different structural furanose isomers based on individual substitution pattern of the hexose molecule. Different isomers may exhibit different affinities to GLUT5 and therefore transport properties. On the other hand,

Molecular Pharmacology Fast Forward. Published on November 15, 2017 as DOI: 10.1124/mol.117.110007
This article has not been copyedited and formatted. The final version may differ from this version.

cellular uptake of 1-[^{18}F]FDF was similar to 2,5-anhydro-D-mannitol derivative 1-[^{18}F]FDAM, a compound with locked furanose-like anomeric conformation. 1-FDAM was developed as an alternative GLUT5 substrate with the potential of intracellular trapping capacity through phosphorylation by hexokinase II (Soueidan et al, 2015). GLUT5-mediated transport of 1-[^{18}F]FDAM was confirmed through inhibition experiments of the radiotracer in the presence of 100mM D-fructose (**Supplemental Figure 1**). Surprisingly both, 1-[^{18}F]FDAM and 1-[^{18}F]FDF, were not substrates of hexokinase II as demonstrated by negative phosphorylation experiments using 2-[^{18}F]FDG as positive control (**Supplemental Figure 1**).

Analysis of different transport inhibition effects revealed that fructose itself blocks glucose uptake into murine and human mammary tumor cells pointing towards functional involvement of other GLUTs beside GLUT5 such as GLUT2. The IC_{50} for fructose was in a similar concentration-range against 6-[^{18}F]FDF uptake (~320mM, Wuest et al. 2011) and glucose uptake (~80 mM in EMT6 and ~220mM in MDA-MB231 cells). Glucose was also able to interfere with 6-[^{18}F]FDF transport, however, with 3 orders of magnitude higher IC_{50} (~120mM against 6-[^{18}F]FDF versus ~0.22mM against glucose). Pointing towards GLUT2 fits well with the reported affinity (K_i) of glucose (~17mM) and 2-FDG (7mM) for GLUT2 (Sala-Rabanal et al. 2016). Uptake of 2-FDG and 6-[^{18}F]FDF into murine and human mammary tumor cells was also blocked pointing towards an additional involvement of another GLUT transporter beside GLUT5. Cytochalasin B is known to inhibit GLUT1-4 but being ineffective to fructose transport through GLUT5 (Chan et al. 2004). Similar observations were reported by Gowrishankar et al. (2011) in human BC MDA-MB468 cells. In addition, we also analyzed effects of a recently described GLUT5

Molecular Pharmacology Fast Forward. Published on November 15, 2017 as DOI: 10.1124/mol.117.110007
This article has not been copyedited and formatted. The final version may differ from this version.

inhibitor MSNBA (George Thompson et al. 2016). Limited by its solubility and the DMSO concentration in the cell assay 300µM MSNBA did only slightly inhibit 6-[^{18}F]FDF uptake into murine BC cells (~25%) while it also influenced 2-[^{18}F]FDG uptake by 15%. According to George Thompson et al. (2016) 60µM MSNBA should lead to a 50% inhibition of fructose uptake into human BC MCF7 cells which we did not observe against 6-[^{18}F]FDF in EMT6 cells indicating that the portion of GLUT5 involvement is very small. Considering that fact, fructose derivative 1-[^{18}F]FDF as well anhydro-mannitol 1-[^{18}F]FDAM show little EMT6 cell uptake which corresponds well to preferential GLUT5 transport only.

PET imaging studies of radiotracers 2-[^{18}F]FDG, 6-[^{18}F]FDG, 1-[^{18}F]FDF, 6-[^{18}F]FDF and 1-[^{18}F]FDAM in EMT6 tumor-bearing mice revealed different uptake patterns *in vivo*. Glucose derivative 2-[^{18}F]FDG showed highest tumor uptake, including metabolic trapping as typical for 2-[^{18}F]FDG as a substrate for GLUT1 and hexokinase II. Lower tumor uptake and no metabolic trapping was observed for 6-[^{18}F]FDG as potential radiotracer for glucose-transport only. Among all radiotracers tested, 1-[^{18}F]FDF and 1-[^{18}F]FDAM showed lowest tumor uptake resulting in overall poor image contrast. Fructose derivative 6-[^{18}F]FDF displayed 2x higher tumor versus muscle uptake and clearance leading to better image contrast. However, 1-[^{18}F]FDF, 6-[^{18}F]FDF and 1-[^{18}F]FDAM showed also washout from tumor tissue confirming no intracellular trapping through phosphorylation with hexokinase II. This is consistent with observed cellular uptake of all three radiotracers into EMT6 cells and negative phosphorylation experiments with hexokinase II (Wuest et al., 2011; **Supplemental Figure 2**).

Present data confirm 6-[^{18}F]FDF as a suitable radiotracer for molecular imaging of fructose-mediated metabolism in BC. However, high uptake of 6-[^{18}F]FDF into EMT6

Molecular Pharmacology Fast Forward. Published on November 15, 2017 as DOI: 10.1124/mol.117.110007
This article has not been copyedited and formatted. The final version may differ from this version.

tumors despite rather low expression levels of GLUT5 suggests involvement of additional hexose transporters. Inhibition of 2-[^{18}F]FDG and 6-[^{18}F]FDF uptake into EMT6 cells in the presence of D-fructose suggest functional involvement of GLUT2. GLUT2 as a complementary hexose transporter to GLUT1 (glucose transport only) and GLUT5 (fructose transport only), is involved in both, glucose and fructose metabolism. Evidence was reported on a GLUT4 involvement in glucose-mediated transport of 2-[^{18}F]FDG into mouse mammary gland cells 5505 while excluding GLUT2 in that specific model (Moadel et al. 2005). Our current results using EMT6 as well as human MDA-MB231 cells point towards GLUT2 considering fructose-mediated transport. Currentf indings along with literature data on substantial challenge to develop GLUT5 selective molecular probes (Tanasova et al., 2013) and insufficient expression of GLUT5 in human BC tissue (Gowrishankar et al., 2011) point to involvement of additional biomarkers like GLUT2 for targeting fructose-metabolism in BC and other malignancies.

In conclusion, our results highlight the importance of detailed biochemical studies on GLUT expression levels in combination with PET imaging studies for functional characterization of GLUTs as biomarkers in BC as e.g. a solely involvement of GLUT5 in fructose-mediated transport does not seem to represent the entire picture. Future studies should include experiments to elucidate detailed functional role of GLUT2 as an additional biomarker for fructose metabolism in BC.

Molecular Pharmacology Fast Forward. Published on November 15, 2017 as DOI: 10.1124/mol.117.110007
This article has not been copyedited and formatted. The final version may differ from this version.

Acknowledgments

The authors would like to thank John Wilson, David Clendening and Blake Lazurko from the Edmonton PET Center for ^{18}F production and excellent technical support. We thank Dan McGinn from the Vivarium of the Cross Cancer Institute for supporting the animal work, Dr. Hans-Soenke Jans from the Division of Medical Physics for technical support of the animal imaging facility (Department of Oncology, University of Alberta).

Autorship contributions

Conception and design: M. Wuest, F. West, C. Cheeseman, F. Wuest

Development of methodology: M. Wuest, I. Hamann, F. Wuest

Acquisition of data: M. Wuest, I. Hamann, V. Bouvet, D. Glubrecht, B. Trayner, A. Marshall, D. Krys

Analysis and interpretation of data: M. Wuest, I. Hamann, F. Wuest

Writing, review and/or revision of the manuscript: M. Wuest, I. Hamann, F. West, C. Cheeseman, F. Wuest

Contributed chemical and radiochemical syntheses: O. Soueidan, V. Bouvet, M. Wagner

Footnotes

Ingrit Hamann thanks the Alberta Cancer Foundation (ACF) for a postdoctoral fellowship award. We also gratefully acknowledge the Dianne and Irving Kipnes Foundation, the Canadian Institute of Health Research (CIHR), the Canadian Breast Cancer Foundation (CBCF), the Collaborative Health Research Program (CHRP) and

Molecular Pharmacology Fast Forward. Published on November 15, 2017 as DOI: 10.1124/mol.117.110007
This article has not been copyedited and formatted. The final version may differ from this version.

the National Science and Engineering Research Council of Canada (NSERC) for supporting this work.

Molecular Pharmacology Fast Forward. Published on November 15, 2017 as DOI: 10.1124/mol.117.110007
This article has not been copyedited and formatted. The final version may differ from this version.

References

Adejolu M, Huo L, Rohren E, Santiago L, Yang WT (2012) False-positive lesions mimicking breast cancer on FDG PET and PET/CT. AJR Am J Roentgenol **198:**W304-314.

Avril N, Menzel M, Dose J, Schelling M, Weber W, Jänicke F, Nathrath W, Schwaiger M (2001) Glucose metabolism of breast cancer assessed by ^{18}F-FDG PET: histologic and immunohistochemical tissue analysis. J Nucl Med **42:**9-16.

Barron CC, Bilan PJ, Tsakiridis T, Tsiani E (2016) Facilitative glucose transporters: Implications for cancer detection, prognosis and treatment. Metabolism **65:**124-139.

Bouvet V, Wuest M, Wiebe LI, Wuest F (2011) Synthesis of hypoxia imaging agent 1-(5-deoxy-5-fluoro-α-D-arabinofuranosyl)-2-nitroimidazole ([^{18}F]FAZA) using microfluidic technology. Nucl Med Biol **38:**235-245.

Brown RS, Leung JY, Fisher SJ, Frey KA, Ethier SP, Wahl RL (1996) Intratumoral distribution of tritiated-FDG in breast carcinoma: correlation between Glut-1 expression and FDG uptake. J Nucl Med **37:**1042-1047.

Chan KK, Chan JY, Chung KK, Fung KP (2004) Inhibition of cell proliferation in human breast tumor cells by antisense oligonucleotides against facilitative glucose transporter 5. J Cell Biochem **93:**1134-1142.

Chudgar AV, Mankoff DA (2017) Molecular Imaging and Precision Medicine in Breast Cancer. PET Clin **12:**39-51.

Dalm SU, Verzijlbergen JF, De Jong M. Review: Receptor Targeted Nuclear Imaging of Breast Cancer (2017) Int J Mol Sci **18:** E260.

Gallamini A, Zwarthoed C, Borra A (2014) Positron Emission Tomography (PET) in Oncology. Cancers (Basel) **6:**1821-1889.

George Thompson AM, Ursu O, Babkin P, Iancu CV, Whang A, Oprea TI, Choe JY (2016) Discovery of a specific inhibitor of human GLUT5 by virtual screening and in vitro transport evaluation. Sci Rep **6:**24240.

Godoy A, Ulloa V, Rodríguez F, Reinicke K, Yañez AJ, García Mde L, Medina RA, Carrasco M, Barberis S, Castro T, Martínez F, Koch X, Vera JC, Poblete MT, Figueroa CD, Peruzzo B, Pérez F, Nualart F (2006) Differential subcellular distribution of glucose transporters GLUT1-6 and GLUT9 in human cancer: ultrastructural localization of GLUT1 and GLUT5 in breast tumor tissues. J Cell Physiol **207:**214-627.

Gowrishankar G, Zitzmann-Kolbe S, Junutula A, Reeves R, Levi J, Srinivasan A, Bruus-Jensen K, Cyr J, Dinkelborg L, Gambhir SS (2011) GLUT 5 is not over-expressed in breast cancer cells and patient breast cancer tissues. PLoS One **6:**e26902.

Haradahira T, Tanaka A, Maeda M, Kanazawa Y, Ichiya YI, Masuda K (1995) Radiosynthesis, rodent biodistribution, and metabolism of 1-deoxy-1-[^{18}F]fluoro-D-fructose. Nucl Med Biol **22:**719-725.

Humbert O, Cochet A, Coudert B, Berriolo-Riedinger A, Kanoun S, Brunotte F, Fumoleau P (2015) Role of positron emission tomography for the monitoring of response to therapy in breast cancer. Oncologist **20:**94-104.

Hwa JS, Kim HJ, Goo BM, Park HJ, Kim CW, Chung KH, Park HC, Chang SH, Kim YW, Kim DR, Cho GJ, Choi WS, Kang KR (2006) The expression of ketohexokinase is diminished in human clear cell type of renal cell carcinoma. Proteomics **6:**1077-1084.

Jadvar H, Alavi A, Gambhir SS (2009) ^{18}F-FDG uptake in lung, breast, and colon cancers: molecular biology correlates and disease characterization. J Nucl Med **50:**1820-1827.

Jameson JL, Longo DL (2015) Precision medicine--personalized, problematic, and promising. N Engl J Med 372: 2229-2234.

Kelly CJ, Hussien K, Muschel RJ (2012) 3D tumour spheroids as a model to assess the suitability of [18F]FDG-PET as an early indicator of response to PI3K inhibition. Nucl Med Biol **39:**986-992.

Kenny L (2016) The Use of Novel PET Tracers to Image Breast Cancer Biologic Processes Such as Proliferation, DNA Damage and Repair, and Angiogenesis. J Nucl Med **57 Suppl 1:** 89S-95S.

Kitajima K, Miyoshi Y (2016) Present and future role of FDG-PET/CT imaging in the management of breast cancer. Jpn J Radiol **34:**167-180.

Knight JC, Wuest M, Saad FA, Wang M, Chapman DW, Jans HS, Lapi SE, Kariuki BM, Amoroso AJ, Wuest F (2013) Synthesis, characterisation and evaluation of a novel copper-64 complex with selective uptake in EMT6 cells under hypoxic conditions Dalton Trans **42:**12005-12014.

Kurihara H, Shimizu C, Miyakita Y, Yoshida M, Hamada A, Kanayama Y, Yonemori K, Hashimoto J, Tani H, Kodaira M, Yunokawa M, Yamamoto H, Watanabe Y, Fujiwara Y, Tamura K (2016) Molecular imaging using PET for breast cancer. Breast Cancer **23:**24-32.

Kuo SJ, Wu YC, Chen CP, Tseng HS, Chen DR (2006) Expression of glucose transporter-1 in Taiwanese patients with breast carcinoma – a preliminary report. Kaohsiung J Med Sci **22:**339-345.

Laudanski P, Koda M, Kozłowski L, Swiatecka J, Wojtukiewicz M, Sulkowski S, Wołczyński S (2004) Expression of glucose transporter GLUT-1 and estrogen receptors ER-alpha and ER-beta in human breast cancer. Neoplasma **51:**164-168.

Lebron L, Greenspan D, Pandit-Taskar N (2015) PET Imaging of Breast Cancer: Role in Patient Management. PET Clin **10:**159-195.

Levi J, Cheng Z, Gheysens O, Patel M, Chan CT, Wang Y, Namavari M, Gambhir SS (2007) Fluorescent fructose derivatives for imaging breast cancer cells. Bioconjug Chem **18:**628-634.

Livak KJ, Schmittgen TD (2001) Analysis of relative gene expression data using real-time quantitative PCR and the 2(-Delta Delta C(T)) Method. Methods **25:**402-408.

Macheda ML, Rogers S, Best JD (2005) Molecular and cellular regulation of glucose transporter (GLUT) proteins in cancer. J Cell Physiol **202:**654-662.

Manolescu AR, Witkowska K, Kinnaird A, Cessford T, Cheeseman C (2007) Facilitated Hexose Transporters: New Perspectives on Form and Function. Physiology **22:**234-240.

Moadel RM, Weldon RH, Katz EB, Lu P, Mani J, Stahl, M, Blaufox MD, Pestell RG, Charron MJ, Dadachova E (2005) Positherapy; Targeted Nuclear Therapy of Breast Cancer with ^{18}F-2-Deoxy-Fluoro-D-Glucose. Cancer Res **65:**698-702.

Neal TR, Schumann WC, Berridge MS, Landau BR (2005) Synthesis of [18F]-6-deoxy-fluoro-D-glucose ([^{18}F]6FDG), a potential tracer of glucose transport. J Label Compd **48:** 845–854.

Niu B, Wen X, Jia Z, Wu X, Guo W, Sun H (2013) Synthesis and preliminary evaluation of 1-[^{18}F]fluoro-1-deoxy-2,5-anhydro-*D*-mannitol as a PET radiotracer for breast cancer imaging. Chin J Chem **31:**1159-1163.

Oude Munnink TH, Nagengast WB, Brouwers AH, Schröder CP, Hospers GA, Lub-de Hooge MN, van der Wall E, van Diest PJ, de Vries EG (2009) Molecular imaging of breast cancer. Breast **18(Suppl3):**S66-73.

Pfaffl MW (2001) A new mathematical model for relative quantification in real-time RT-PCR. Nucleic Acids Res **29:**e45.

Ravazoula P, Batistatou A, Aletra C, Ladopoulos J, Kourounis G, Tzigounis B (2003) Immunohistochemical expression of glucose transporter Glut1 and cyclin D1 in breast carcinomas with negative lymph nodes. Eur J Gynaecol Oncol **24:**544-546.

Rowland DJ, Garbow JR, Laforest R, Snyder AZ (2005) Registration of [18F]FDG microPET and small-animal MRI. Nucl Med Biol **32:**567-572.

Sala-Rabanal M, Hirayama BA, Ghezzi C, Liu J, Huang SC, Kepe V, Koepsell H, Yu A, Powell DR, Thorens B, Wright EM, Barrio JR (2016) Revisiting the physiological roles of SGLTs and GLUTs using positron emission tomography in mice. J Physiol **594:**4425-4438.

Siegel RL, Miller KD, Jemal A (2017) Cancer Statistics 2017. CA Cancer J Clin **67:**7-30.

Soule HD, Maloney TM, Wolman SR, Peterson WD Jr, Brenz R, McGrath CM, Russo J, Pauley RJ, Jones RF, Brooks SC (1990) Isolation and characterization of a spontaneously immortalized human breast epithelial cell line, MCF-10 Cancer Res **50:**6075-6086.

Molecular Pharmacology Fast Forward. Published on November 15, 2017 as DOI: 10.1124/mol.117.110007
This article has not been copyedited and formatted. The final version may differ from this version.

Soueidan OM, Trayner BJ, Grant TN, Henderson JR, Wuest F, West FG, Cheeseman CI (2015) New fluorinated fructose analogs as selective probes of the hexose transporter protein GLUT5. Org Biomol Chem **13:**6511-6521.

Soueidan OM, Scully TW, Kaur J, Panigrahi R, Belovodskiy A, Do V, Matier CD, Lemieux MJ, Wuest F, Cheeseman C, West FG (2017) Fluorescent Hexose Conjugates Establish Stringent Stereochemical Requirement by GLUT5 for Recognition and Transport of Monosaccharides. ACS Chem Biol. doi:10.1021/acschembio.6b01101.

Tanasova M, Plutschack M, Muroski ME, Sturla SJ, Strouse GF, McQuade DT (2013) Fluorescent THF-based fructose analogue exhibits fructose-dependent uptake. Chembiochem **14:**1263-1270.

Tian Q, Stepaniants SB, Mao M, Weng L, Feetham MC, Doyle MJ, Yi EC, Dai H, Thorsson V, Eng J, Goodlett D, Berger JP, Gunter B, Linseley PS, Stoughton RB, Aebersold R, Collins SJ, Hanlon WA, Hood LE (2004) Integrated genomic and proteomic analyses of gene expression in Mammalian cells. Mol Cell Proteomics **10:**960-969.

Trayner BJ, Grant TN, West FG, Cheeseman CI (2009) Synthesis and characterization of 6-deoxy-6-fluoro-D-fructose as a potential compound for imaging breast cancer with PET. Bioorg Med Chem **7:**5488-5495.

Ulaner GA, Riedl CC, Dickler MN, Jhaveri K, Pandit-Taskar N, Weber W (2016) Molecular Imaging of Biomarkers in Breast Cancer. J Nucl Med **57(Suppl 1):**53S-59S.

Way JD, Wang M, Hamann I, Wuest M, Wuest F (2014) Synthesis and evaluation of 2-amino-5-(4-[18F]fluorophenyl)pent-4-ynoic acid ([18F]FPhPA): A novel 18F-labeled amino acid for oncologic PET imaging. Nucl Med Biol **41:**660-669.

Molecular Pharmacology Fast Forward. Published on November 15, 2017 as DOI: 10.1124/mol.117.110007
This article has not been copyedited and formatted. The final version may differ from this version.

Wuest M, Trayner BJ, Grant TN, Jans HS, Mercer JR, Murray D, West FG, McEwan AJ, Wuest F, Cheeseman CI (2011) Radiopharmacological evaluation of 6-deoxy-6-[^{18}F]fluoro-D-fructose as a radiotracer for PET imaging of GLUT5 in breast cancer. Nucl Med Biol **38:**461-475.

Wuest M, Kumar P, Wang M, Yang J, Jans HS, Wiebe LI (2012) In vitro and in vivo evaluation of [(18)F]F-GAZ, a novel oxygen-mimetic azomycin-glucose conjugate, for imaging hypoxic tumor. Cancer Biother Radiopharm 27:473-780.

Wuest M, Kuchar M, Sharma SK, Richter S, Hamann I, Wang M, Vos L, Mackey JR, Wuest F, Löser R (2015) Targeting lysyl oxidase for molecular imaging in breast cancer. Breast Cancer Res 17:107.

Yamamoto T, Seino Y, Fukumoto H, Koh G, Yano H, Inagaki N, Yamada Y, Inoue K, Manabe T, Imura H (1990) Over-expression of facilitative glucose transporter genes in human cancer. Biochem Biophys Res Commun **170:**223-230.

Younes M, Brown RW, Mody DR, Fernandez L, Laucirica R (1990) GLUT1 expression in human breast carcinoma: correlation with known prognostic markers. Anticancer Res **15:**2895-2898.

Zamora-León SP, Golde DW, Concha II, Rivas CI, Delgado-López F, Baselga J, Nualart F, Vera JC (1996) Expression of the fructose transporter GLUT5 in human breast cancer. Proc Natl Acad Sci U S A **93:**1847-1852.

Molecular Pharmacology Fast Forward. Published on November 15, 2017 as DOI: 10.1124/mol.117.110007
This article has not been copyedited and formatted. The final version may differ from this version.

Figure legends

Figure 1 Chemical structures of ^{18}F-labeled glucose, fructose and 2,5-anhydro-D-mannitol derivatives

Figure 2 **A)** Inhibition of 6-[^{18}F]FDF uptake into EMT6 cells using non-radiolabeled fructose and 2,5-anhydro-D-mannitol derivatives 1-FDF, 3-FDF, 6-FDF and 1-FDAM in comparison to fructose. **B)** Cellular uptake of radiolabeled glucose, fructose and 2,5-anhydro-D-mannitol derivatives 2-[^{18}F]FDG, 6-[^{18}F]FDG 1-[^{18}F]FDF, 6-[^{18}F]FDF and 1-[^{18}F]FDAM into EMT6 cells over 60 min. **C)** Inhibitory effect of fructose on 2-[^{18}F]FDG uptake in EMT6 and MDA-MB231 cells as well as concentration-dependent inhibition with cytochalasin B (GLUT1, GLUT2, GLUT4 inhibitor) in MDA-MB231 cells in comparison to the effect of glucose on 2-[^{18}F]FDG in EMT6 cells (*data from Wuest et al., 2012). **D)** Inhibitory effect of glucose on 6-[^{18}F]FDF uptake in MDA-MB231 cells. **E)** Comparison of cellular uptake of 2-[^{18}F]FDG and 6-[^{18}F]FDF into murine EMT6 and human MDA-MB231 cells after 60 min incubation. **F)** Comparison of the inhibitory effect of 30 μM cytochalasin B on 2-[^{18}F]FDG and 6-[^{18}F]FDF in MDA-MB231 and EMT6 cells after 60 min incubation. **G)** and **H)** Inhibitory effect of GLUT5 blocker MSNBA on 2-[^{18}F]FDG (in comparison to glucose) and on 6-[^{18}F]FDF (in comparison to fructose). All data are shown as mean ± SEM from n experiments. *p<0.05; ***p<0.001.

Figure 3 Relative GLUT mRNA profiles in EMT6 tumor tissue (A, *left*) and mouse muscle tissue (A, *right*) and differences in relative GLUT 1 and GLUT 5 mRNA levels between EMT6 tumor tissue and mouse muscle tissue (B, *bottom*) were

Molecular Pharmacology Fast Forward. Published on November 15, 2017 as DOI: 10.1124/mol.117.110007
This article has not been copyedited and formatted. The final version may differ from this version.

determined in RT-PCR analyses using specific Taqman assays, normalized against 18 S RNA. Data are shown as mean ± SEM from n experiments.

Figure 4 Quantitative comparison of GLUT 5 protein levels in EMT6 tumor and mouse muscle tissue, using western blot analyses. A) Western blot analysis; B) relative GLUT 5 protein analysis normalized to GLUT5 levels in tumor tissue Data are shown as mean ± SEM from n experiments.; C) absolute data for each animal: comparison of GLUT5 in tumor and muscle tissue.

Figure 5 Immunohistochemical staining of GLUT 5 in mouse intestine (positive control), mouse muscle and EMT6 tumor tissue. Pictures were taken using a 20x objective.

Figure 6 PET images of 1-[^{18}F]FDF, 6-[^{18}F]FDF, 1-[^{18}F]FDAM, 2-[^{18}F]FDG and 6-[^{18}F]FDG after 15 min (*top*) and 60 min (*bottom*) p.i. of 5-7 MBq of the radiotracer into EMT6 tumor bearing mice. Images are shown as maximum intensity projections (MAP). SUV values at 15 and 60 min p.i. are included as mean ± SEM from n experiments. Tumors are delineated in the images.

Figure 7 Time-activity curves (TACs) for EMT6 tumor and muscle tissue uptake profile for 1-[^{18}F]FDF, 6-[^{18}F]FDF, 1-[^{18}F]FDAM, 2-[^{18}F]FDG and 6-[^{18}F]FDG over 2 h p.i. *bottom right*: TACs for the subsequent calculated tumor-to-muscle ratios for each radiotracer investigated. TACs are presented as semi-quantitative standardized uptake values (SUV) and mean ± SEM from n experiments. *p<0.05; **p<0.01.

Molecular Pharmacology Fast Forward. Published on November 15, 2017 as DOI: 10.1124/mol.117.110007
This article has not been copyedited and formatted. The final version may differ from this version.

A) Radiolabeled glucose derivatives

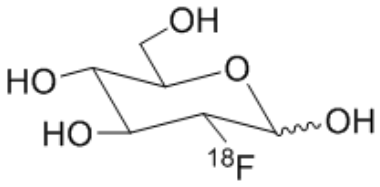

2-[^{18}F]FDG

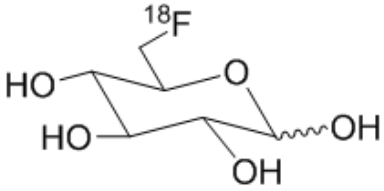

6-[^{18}F]FDG

B) Radiolabeled fructose derivatives

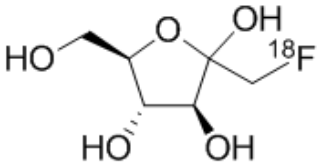

1-[^{18}F]FDF

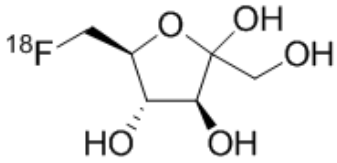

6-[^{18}F]FDF

C) Radiolabeled mannose derivative

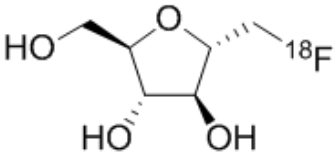

1-[^{18}F]FDAM

Figure 1

Molecular Pharmacology Fast Forward. Published on November 15, 2017 as DOI: 10.1124/mol.117.110007
This article has not been copyedited and formatted. The final version may differ from this version.

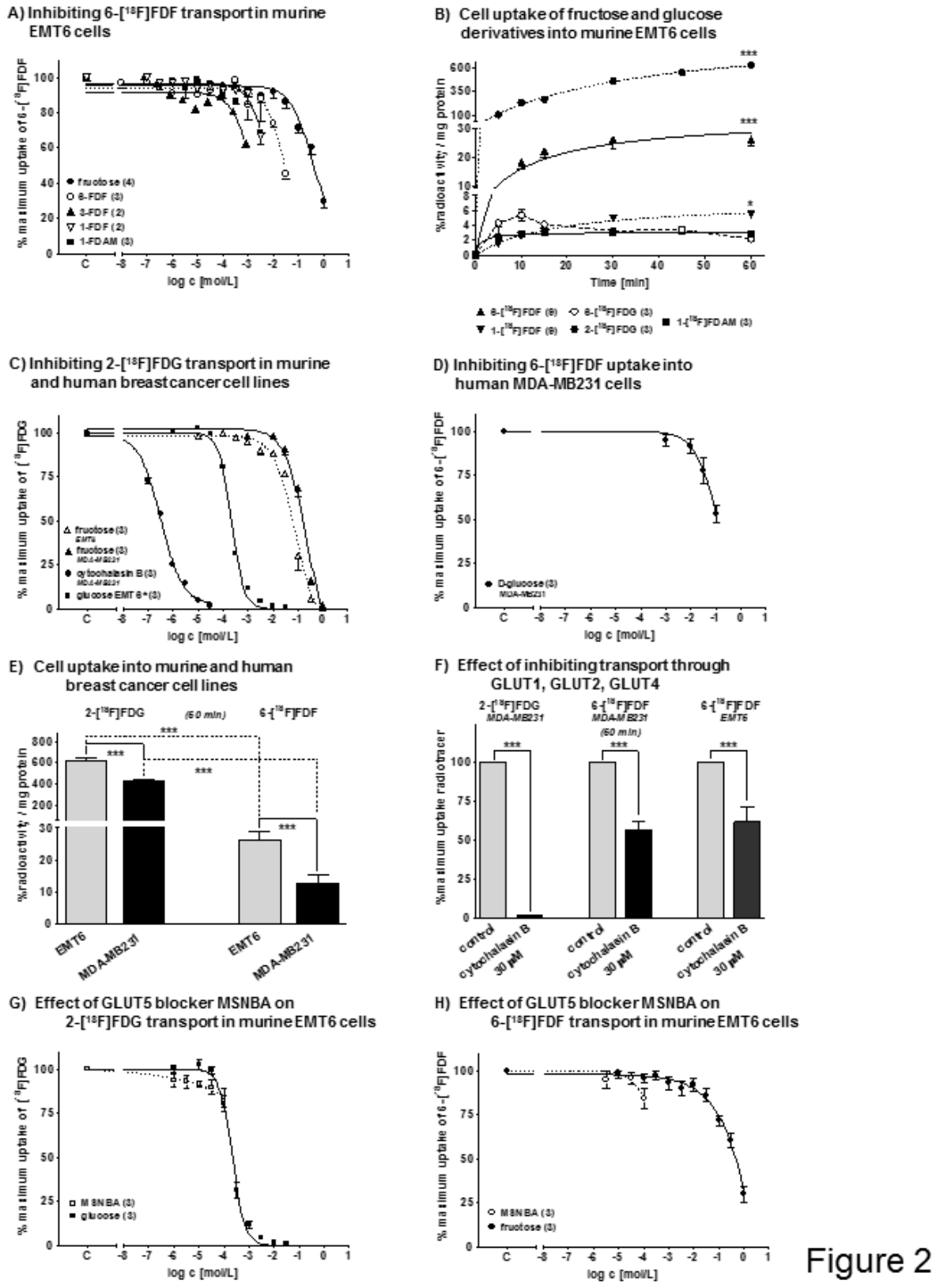

Figure 2

Molecular Pharmacology Fast Forward. Published on November 15, 2017 as DOI: 10.1124/mol.117.110007
This article has not been copyedited and formatted. The final version may differ from this version.

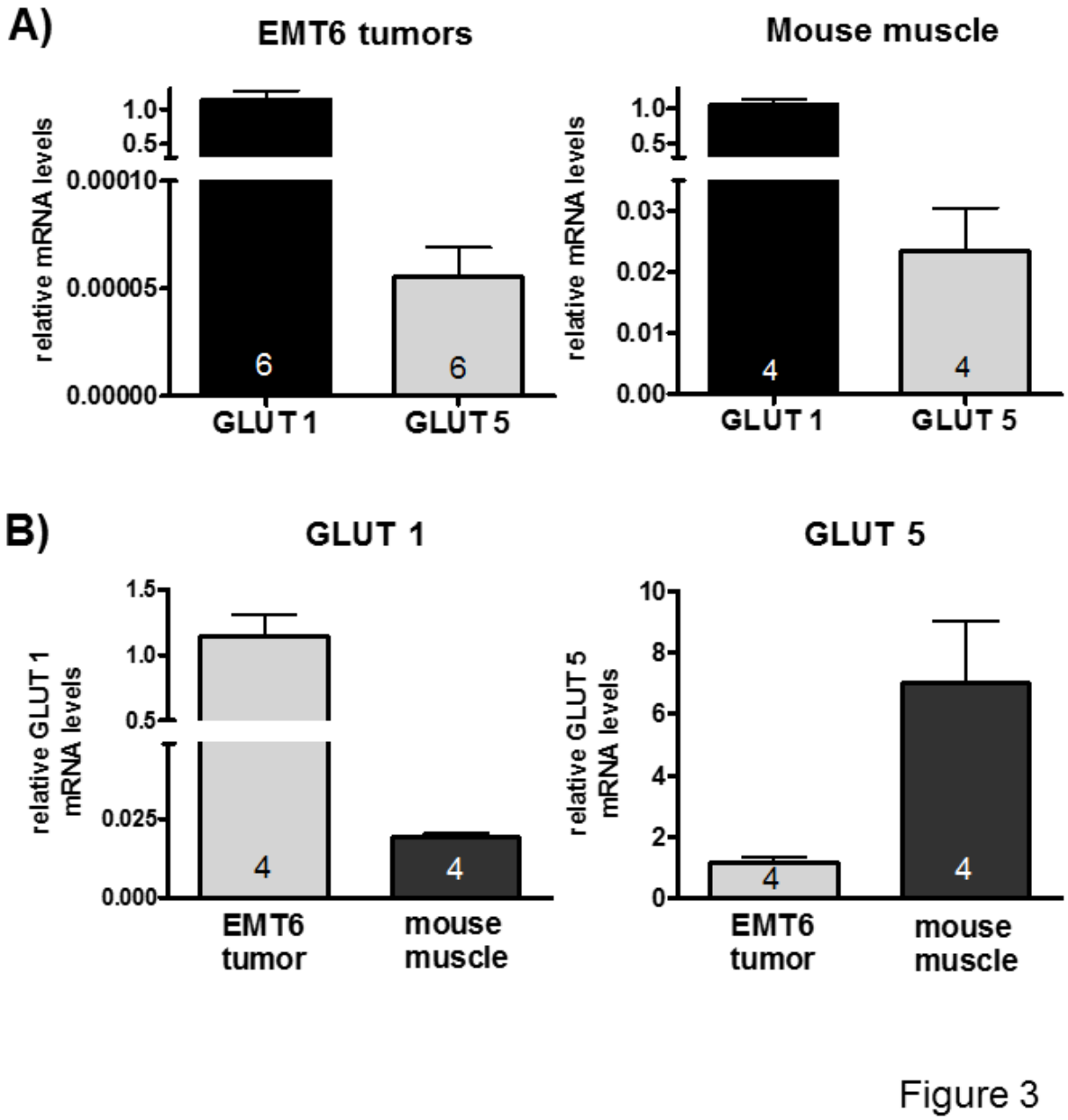

Figure 3

Molecular Pharmacology Fast Forward. Published on November 15, 2017 as DOI: 10.1124/mol.117.110007
This article has not been copyedited and formatted. The final version may differ from this version.

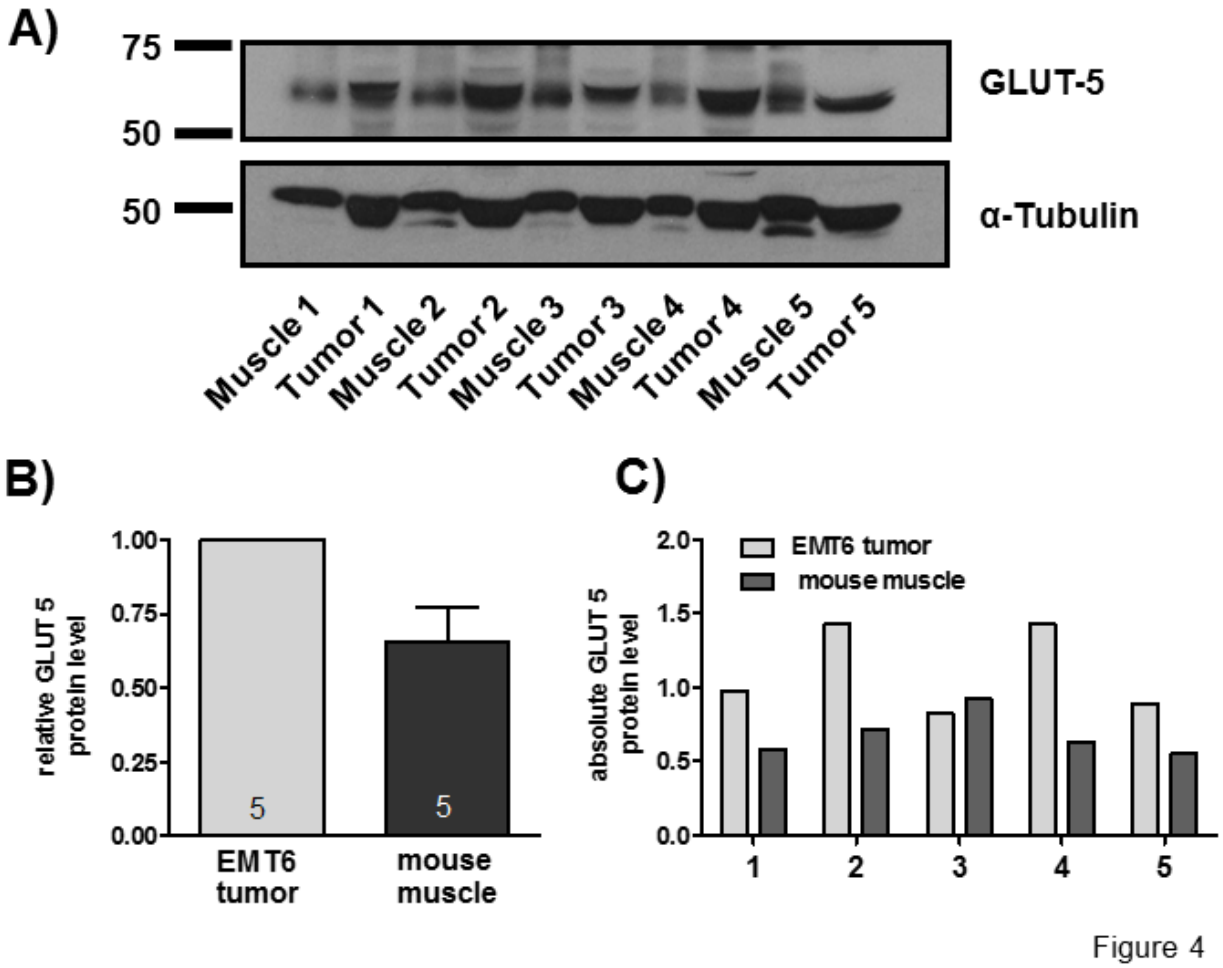

Figure 4

Molecular Pharmacology Fast Forward. Published on November 15, 2017 as DOI: 10.1124/mol.117.110007
This article has not been copyedited and formatted. The final version may differ from this version.

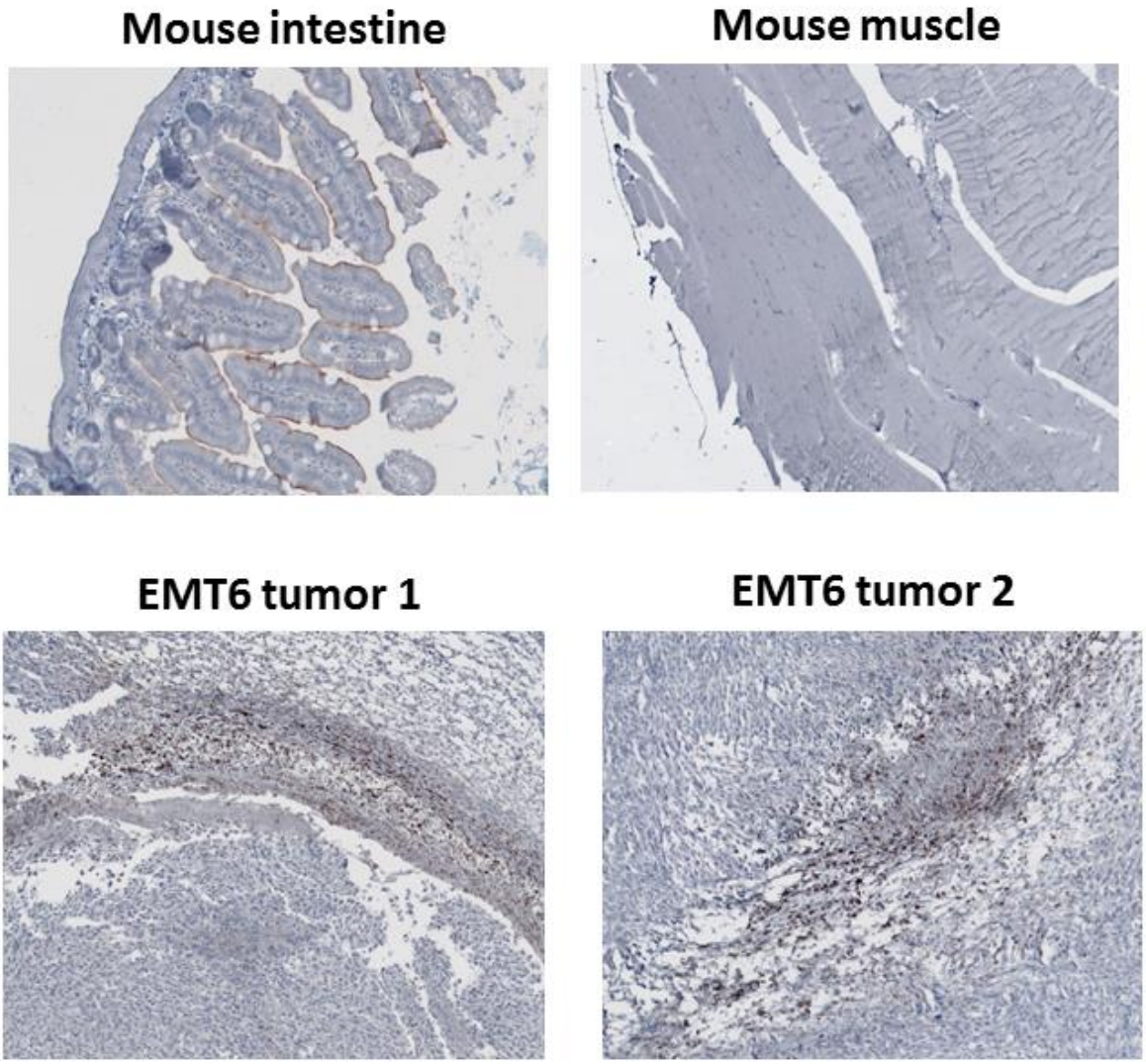

Figure 5

Molecular Pharmacology Fast Forward. Published on November 15, 2017 as DOI: 10.1124/mol.117.110007
This article has not been copyedited and formatted. The final version may differ from this version.

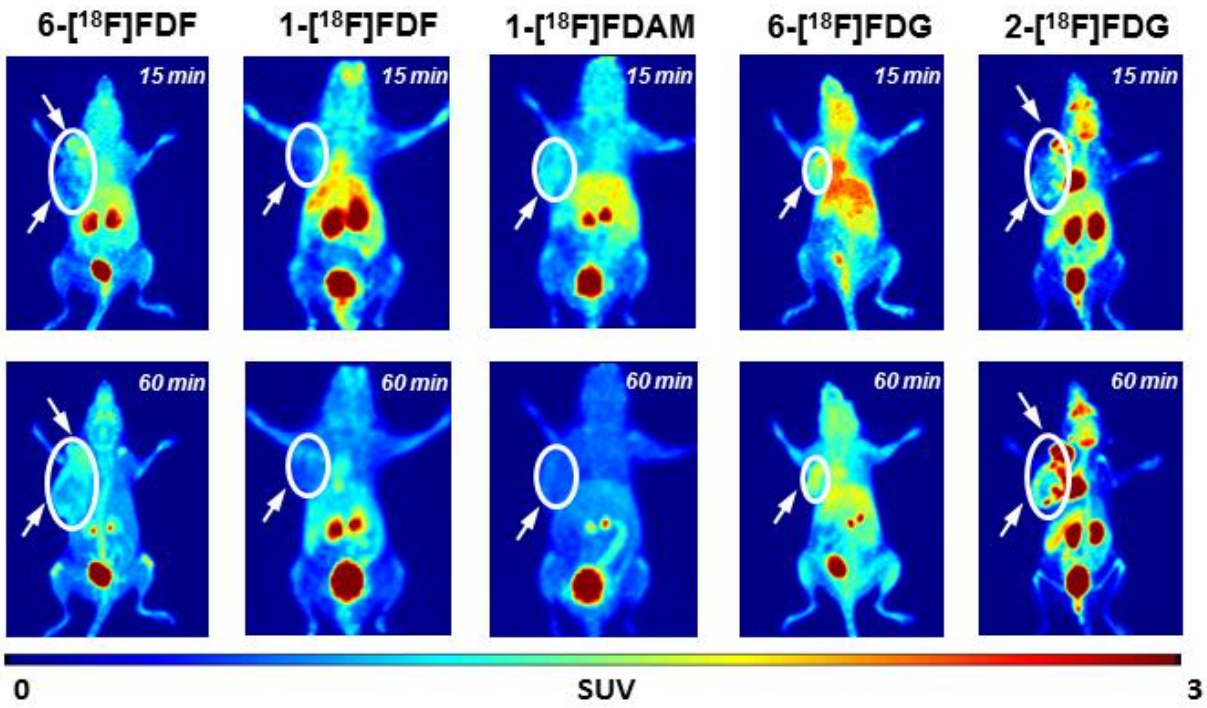

Figure 6

Molecular Pharmacology Fast Forward. Published on November 15, 2017 as DOI: 10.1124/mol.117.110007
This article has not been copyedited and formatted. The final version may differ from this version.

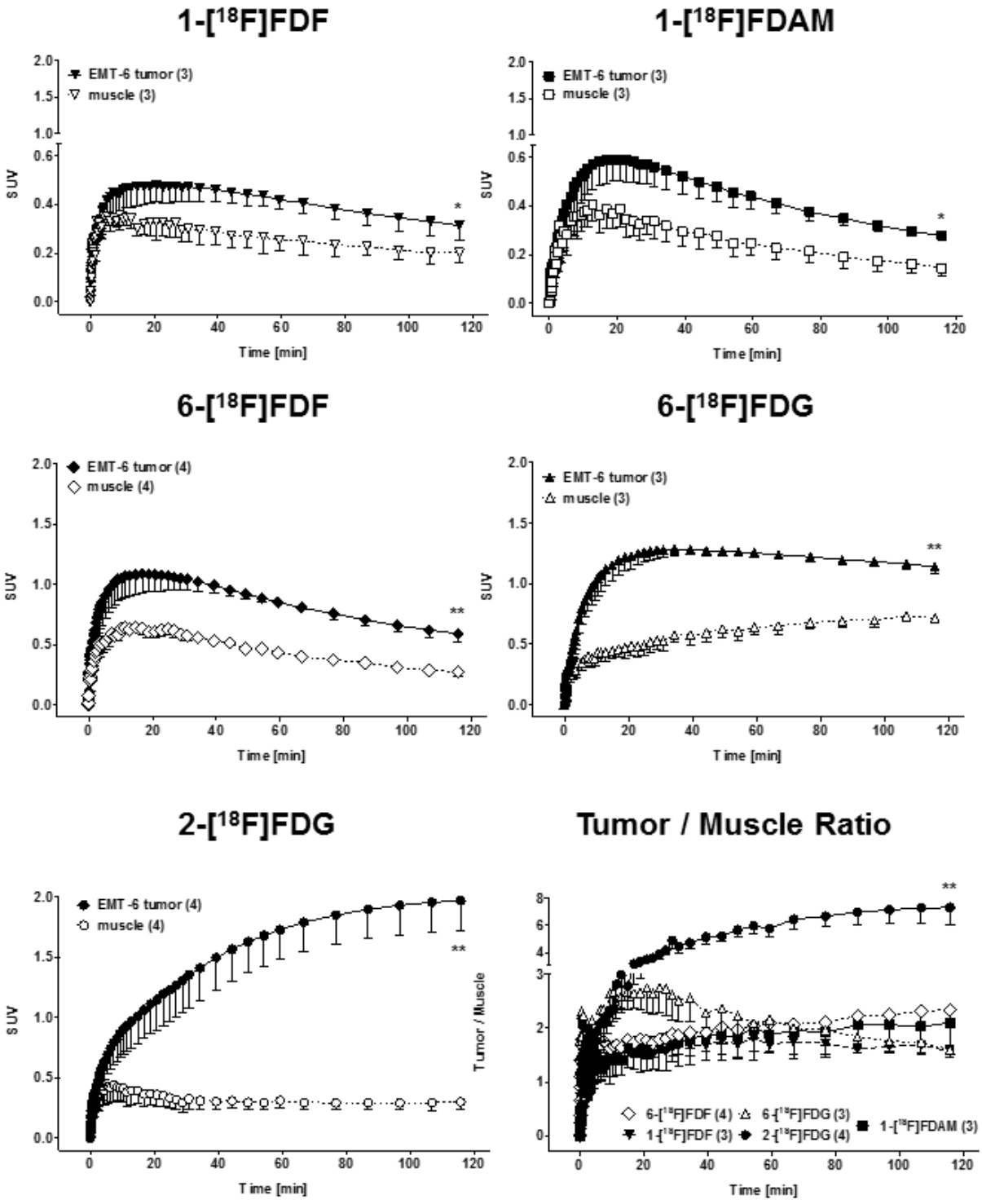

Figure 7